

Temporal patterns of synchrony in a pyramidal-interneuron gamma (PING) network

Cite as: Chaos 31, 043134 (2021); doi: 10.1063/5.0042451

Submitted: 30 December 2020 · Accepted: 5 April 2021 ·

Published Online: 22 April 2021




View Online



Export Citation



CrossMark

Quynh-Anh Nguyen¹  and Leonid L. Rubchinsky^{1,2,a)} 

AFFILIATIONS

¹Department of Mathematical Sciences, Indiana University Purdue University Indianapolis, Indianapolis, Indiana 46202, USA

²Stark Neurosciences Research Institute, Indiana University School of Medicine, Indianapolis, Indiana 46202, USA

^{a)}Author to whom correspondence should be addressed: lrubchin@iupui.edu

ABSTRACT

Synchronization in neural systems plays an important role in many brain functions. Synchronization in the gamma frequency band (30–100 Hz) is involved in a variety of cognitive phenomena; abnormalities of the gamma synchronization are found in schizophrenia and autism spectrum disorder. Frequently, the strength of synchronization is not high, and synchronization is intermittent even on short time scales (few cycles of oscillations). That is, the network exhibits intervals of synchronization followed by intervals of desynchronization. Neural circuit dynamics may show different distributions of desynchronization durations even if the synchronization strength is fixed. We use a conductance-based neural network exhibiting pyramidal-interneuron gamma rhythm to study the temporal patterning of synchronized neural oscillations. We found that changes in the synaptic strength (as well as changes in the membrane kinetics) can alter the temporal patterning of synchrony. Moreover, we found that the changes in the temporal pattern of synchrony may be independent of the changes in the average synchrony strength. Even though the temporal patterning may vary, there is a tendency for dynamics with short (although potentially numerous) desynchronizations, similar to what was observed in experimental studies of neural synchronization in the brain. Recent studies suggested that the short desynchronizations dynamics may facilitate the formation and the breakup of transient neural assemblies. Thus, the results of this study suggest that changes of synaptic strength may alter the temporal patterning of the gamma synchronization as to make the neural networks more efficient in the formation of neural assemblies and the facilitation of cognitive phenomena.

Published under an exclusive license by AIP Publishing. <https://doi.org/10.1063/5.0042451>

Synchronization of neural oscillations is a common neural phenomenon believed to be relevant to a large range of neural functions and dysfunctions. Neural synchrony at rest is rarely perfect and fluctuates in time. Few long desynchronizations and many short desynchronizations may lead to different functional consequences even if the average synchrony strength is not changed. This study explores the potential network mechanisms of different temporal patterns of neural synchrony in the model of synchronized neural gamma oscillations, which are related to cognitive function of the brain. The study shows how gamma rhythm can be partially synchronized with specific temporal patterning, and how this temporal patterning of gamma synchronization is regulated by connectivity strength and other factors. Furthermore, the study shows how temporal patterning of neural synchronization can be varied independently of the synchrony strength. Understanding the mechanisms of temporal patterning of neural synchrony may help to understand its relation to neural function.

I. INTRODUCTION

Synchronization in neural networks is a widespread phenomenon that is important for a variety of brain functions and dysfunctions. Through synchrony, collective behavior in neural networks can be established; thus, synchrony may play an important role in memory, cognition, and perception (e.g., [Buzsáki and Draguhn, 2004](#) and [Buzsáki, 2006](#)). Abnormal synchrony is found to be associated with different brain disorders such as Parkinson's disease ([Hammond et al., 2007](#); [Oswal et al., 2013](#); and [Rubchinsky et al., 2012](#)), schizophrenia ([Uhlhaas and Singer, 2010](#); [Pittman-Polletta et al., 2015](#); and [Spellman and Gordon, 2015](#)), and autism ([Sun et al., 2012](#) and [Malaia et al., 2020](#)). Synchronization in the gamma frequency band is a focus of many studies as it is believed to be responsible for the facilitation of interneuronal communication for cognition ([Fries, 2015](#)).

Synchronization in the brain networks is not a perfect synchronization, at least not at the rest state. While this may be affected by many factors, when a network shows a moderate synchrony

strength, it goes in and out of the synchronized state. Networks with similar synchrony strength can have a completely different temporal synchrony pattern. One can have many brief desynchronization events or a few long desynchronization events even if the synchrony strength is the same. Given the importance of synchrony in the brain for behavior, the temporal patterning of synchrony on short time scales should be important.

Techniques to detect and analyze the temporal patterning of synchronous dynamics were recently developed (Park *et al.*, 2010 and Ahn *et al.*, 2011), using the first-return maps for the phases of oscillations. These techniques were applied to experimental data (e.g., Park *et al.*, 2010; Ahn and Rubchinsky, 2013; 2014; Ratnadurai-Giridharan *et al.*, 2016; Malaia *et al.*, 2020; and Dos Santos Lima *et al.*, 2020); it was found that the patterning of neural synchrony (even if the overall synchrony strength is not changed) may be correlated with behavior (Ahn *et al.*, 2014; 2018 and Malaia *et al.*, 2020). One of the interesting observations of all these studies was that the temporal patterning of synchronization was very specific: oscillations go out of synchrony predominantly for a very short amount of time (although they may do so rarely or frequently resulting in high or low overall synchrony).

In the present study, we use these analysis techniques to investigate the temporal patterning of synchronization in the gamma frequency band. We consider a model of two connected circuits exhibiting a pyramidal-interneuron gamma (PING) rhythm. The properties of the gamma rhythm in these circuits rely upon synaptic time scales and synaptic strength of excitatory and inhibitory connections (e.g., Ementrout and Kopell, 1998; Buzsáki and Wang, 2012; and Borgers, 2017). We hypothesize that inhibitory and excitatory synaptic connections do not only change gamma oscillations and their synchrony level but also alter the temporal pattern of synchrony. While the network we use may be viewed as a somewhat simplistic representation of a gamma rhythm in the brain, our objective is to see if and how synaptic and cellular properties may potentially affect the temporal structure of synchrony as a proof of principle. We found that the temporal patterning of synchrony can be changed by the synaptic and cellular changes and can even be altered independently of the overall synchrony strength. We further conclude with the discussion of the modeling results in the context of the available experimental analysis of the temporal patterning of neural synchronization.

II. METHODS

Our network consists of two synaptically connected circuits, each of which generates gamma-band activity in isolation. Each circuit includes two excitatory neurons and two inhibitory neurons and is adapted from Borgers, (2017). Figures 1(a) and 1(b) illustrate the schematic of the network.

A. Model neurons and synapses

Each model neuron is represented by a single compartment conductance-based model (see, e.g., Izhikevich, 2007 and Ermentrout and Terman, 2010). Transmembrane voltage is given by

$$C_m \frac{dV}{dt} = -I_{Na} - I_K - I_L - I_{syn} + I_{app}, \quad (1)$$

with the membrane currents described below. $I_{Na} = g_{Na} m^3 h (V - v_{Na})$ is the transient sodium current. The activation is considered to be instantaneous and m is taken as $m = \alpha_m(V)/(\alpha_m(V) + \beta_m(V))$. The inactivation function h obeys first-order kinetics,

$$\frac{dh}{dt} = \alpha_h(V)(1 - h) - \beta_h(V)h. \quad (2)$$

$I_K = g_K n^4 (V - v_K)$ is the persistent potassium current, and the activation function n obeys first-order kinetics,

$$\frac{dn}{dt} = \alpha_n(V)(1 - n) - \beta_n(V)h. \quad (3)$$

Here, α_* and β_* are probabilities of opening and closing of the corresponding channel, respectively. Finally, $I_L = g_L (V - v_L)$ is the leak current, and I_{app} is a constant applied current.

Excitatory neurons and inhibitory neurons have a different set of parameters and α_* and β_* functions. Excitatory neurons follow the reduced Traub and Miles model (Traub and Miles, 1991) with $C_m = 1 \mu\text{F}/\text{cm}^2$, $v_{Na} = 50 \text{ mV}$, $v_K = -100 \text{ mV}$, $v_L = -67 \text{ mV}$, $g_{Na} = 100 \text{ mS}/\text{cm}^2$, $g_K = 80 \text{ mS}/\text{cm}^2$, and $g_L = 0.1 \text{ mS}/\text{cm}^2$. The $\alpha_*(V)$ and $\beta_*(V)$ functions are given as

$$\alpha_m(V) = \frac{0.32(V+54)}{1 - \exp(-\frac{V+54}{4})} \quad \beta_m(V) = \frac{0.28(V+27)}{\exp(\frac{V+27}{5}) - 1}, \quad (4)$$

$$\alpha_h(V) = 0.128 \exp(-\frac{V+50}{18}) \quad \beta_h(V) = \frac{4}{1 + \exp(-\frac{V+27}{5})}, \quad (5)$$

$$\alpha_n(V) = \frac{0.032(V+52)}{1 - \exp(-\frac{V+52}{5})} \quad \beta_n(V) = 0.5 \exp(-\frac{V+57}{40}). \quad (6)$$

Inhibitory neurons follow the Wang–Buzsáki model (Wang and Buzsáki, 1996) with $C_m = 1 \mu\text{F}/\text{cm}^2$, $v_{Na} = 55 \text{ mV}$, $v_K = -90 \text{ mV}$, $v_L = -65 \text{ mV}$, $g_{Na} = 35 \text{ mS}/\text{cm}^2$, $g_K = 9 \text{ mS}/\text{cm}^2$, and $g_L = 0.1 \text{ mS}/\text{cm}^2$. The $\alpha_*(V)$ and $\beta_*(V)$ functions are given as

$$\alpha_m(V) = \frac{0.1(V+35)}{1 - \exp(-\frac{V+35}{10})} \quad \beta_m(V) = 4 \exp(-\frac{V+60}{18}), \quad (7)$$

$$\alpha_h(V) = 0.35 \exp(-\frac{V+58}{20}) \quad \beta_h(V) = \frac{5}{1 + \exp(-\frac{V+28}{10})}, \quad (8)$$

$$\alpha_n(V) = \frac{0.05(V+34)}{1 - \exp(-\frac{V+34}{10})} \quad \beta_n(V) = 0.625 \exp(-\frac{V+44}{80}). \quad (9)$$

The synaptic current is given as $I_{syn} = g_{syn} s(t) (V_{post} - v_{syn})$. Here, V_{post} is the potential of the postsynaptic cell, v_{syn} is the reverse synaptic potential, and g_{syn} is the synaptic strength. Synaptic gating variable $s(t)$ follows first-order kinetics equation (Izhikevich, 2007 and Ermentrout and Terman, 2010),

$$\frac{ds}{dt} = H(V_{pre}) \frac{1-s}{\tau_r} - \frac{s}{\tau_d}, \quad (10)$$

where $H(V_{pre}) = (1 + \tanh(V_{pre}/4))/2$ is a sigmoidal function of the presynaptic neuron potential V_{pre} and τ_r , τ_d are synaptic rise and synaptic decay time constants, respectively. AMPA-receptor-mediated excitatory synapse has $\tau_r = 0.1 \text{ ms}$, $\tau_d = 3 \text{ ms}$, $v_{syn} = 0 \text{ mV}$. GABA-receptor-mediated inhibitory synapse has $\tau_r = 0.3 \text{ ms}$, $\tau_d = 9 \text{ ms}$, $v_{syn} = -80 \text{ mV}$. These parameters are taken from Borgers *et al.* (2012) and Borgers (2017).

B. Network connectivity

The model is comprised of two circuits with two excitatory neurons (E neurons) and two inhibitory neurons (I neurons) in each circuit. Synaptic connection strength within the circuit is denoted as $g_{syn} = g_*$, and $g_{syn} = c_*$ is connection between the circuit; see Fig. 1. Synaptic connection strength is measured in mS/cm²; for brevity, we will not use the units of measurements when we refer to synaptic strength. It has been pointed out that EE connection should not play a significant role in gamma oscillation (Borgers, 2017 and Ermentrout and Kopell, 1998); thus, we set $g_{EE} = c_{EE} = 0$. All other connections between neurons are included in the model, and there are no recurrent connections.

Within each circuit, there are inhibitory synapses between I neurons as well as from I to E neurons and excitatory synapses from E to I neurons. In the full network (two connected circuits), each E neuron receives inhibitory inputs from two I neurons of the same circuit (g_{IE}) and two I neurons of the other circuit (c_{IE}). Each I cell receives excitatory inputs from two E neurons of the same circuit (g_{EI}) and two E neurons of the other circuit (c_{EI}) and inhibitory inputs from the other I neuron of the same circuit (g_{II}) and two I neurons of the other circuit (c_{II}). The schematic of the model is summarized in Figs. 1(a) and 1(b). The default values for synaptic connections between neurons are $g_{IE} = 0.7$, $g_{EI} = 0.1$, $g_{II} = 0.3$, and $c_{IE} = c_{EI} = c_{II} = 0.02$.

Neurons from each circuit have slightly different values of constant I_{app} so that circuits have slightly different frequencies. In the slower circuit, E neurons have $I_{app} = 4.5$ mA/cm² and 4 mA/cm², while I neurons have $I_{app} = 0.1$ mA/cm² and 0.09 mA/cm². In the faster circuit, E neurons have $I_{app} = 5$ mA/cm² and 4.5 mA/cm², while I neurons have $I_{app} = 0.08$ mA/cm² and 0.07 mA/cm². The slower circuit has a 44.4 Hz average firing rate and the faster circuit has a 46.8 Hz average firing rate.

We vary the strength of different synapses as described below. Some current kinetics parameters are also varied in some numerical simulations as described below. Otherwise, parameters are kept at their default values. The system is solved using the adaptive Runge–Kutta (4,5) method (MATLAB ode45 solver) for 25 s.

C. Time-series analysis

To analyze the dynamics of synchronization between two circuits, we look at the relationship between the phases of oscillators on short time scales (one cycle of oscillations), employing the time-series analysis approach used in earlier experimental studies (Park et al., 2010; Ahn and Rubchinsky, 2013; and Ahn et al., 2014) and computational studies (Ahn and Rubchinsky, 2017) of neural synchrony. We consider the time-series of total synaptic current into a neuron. In each circuit, we choose the excitatory neuron that has a higher firing rate. First, we use Hilbert transform to compute the phase of each time-series, denoted as $\varphi_1(t)$ and $\varphi_2(t)$. Then, the average synchronization index γ (e.g., Pikovsky et al., 2001 and Hurtado et al., 2004) is computed as

$$\gamma = \left\| \frac{1}{N} \sum_{j=1}^N e^{i(\varphi_1(t_j) - \varphi_2(t_j))} \right\|, \quad (11)$$

where $\varphi_1(t_j)$ and $\varphi_2(t_j)$ are the phases of a neuron from circuit 1 (slower circuit) and a neuron from circuit 2 (faster circuit), respectively, at time t_j , N is the number of timepoints, and $\|\cdot\|$ denotes the magnitude of a complex number. The average synchronization index γ varies between 0 (no synchrony) and 1 (full synchrony). For intermediate values of γ , the system is partially synchronized.

We then proceed to characterize the temporal pattern of synchronization. The idea of this approach is first to find the presence of a synchronized state (which requires analysis of long time-series, as synchronization is not an instantaneous phenomenon) and then to track the oscillations on each cycle by checking if they are close to the synchronized state or not. The method for it has been described earlier in Park et al. (2010), Ahn and Rubchinsky (2013; 2017), and Ahn et al. (2014). Briefly, a discrete set of phase difference values $\{\phi_i\}$ is obtained by recording the value of $\varphi_2(t_j)$ whenever $\varphi_1(t_j)$ goes from negative to positive values. For partially synchronized dynamics, these values will cluster around some mean. Note that the mean is not necessarily zero, and thus, this analysis detects not only zero lag synchronization. If $\{\phi_i\}$ is more than $\pi/2$ away from its mean value, the signals are considered to be in the desynchronized state during the cycle i ; otherwise, the signals are considered to be in the synchronized state. The number of consecutive cycles in which the signals are desynchronized is called the duration of desynchronization.

The distribution of desynchronization durations provides a statistical description of the temporal patterning of synchronized dynamics. Examples of desynchronization durations distributions are shown in panels E, F, and G of Figs. 2–10, where the horizontal axis in histograms measures the duration of desynchronizations in the number of cycles of oscillations. The number of desynchronization durations in each histogram usually varies around 300–600. Following earlier studies of these temporal patterns, we will use mode and a desynchronization ratio, as well as the average desynchronization duration. The mode tells us the most common desynchronization duration, and f_{mode} measures how frequent the modal value is. The value of f_{mode} describes how much the system favors the most typical synchronizations; values closer to 1 show that most of the desynchronizations last as long as their mode. The desynchronization ratio is defined as the ratio of the relative frequency of desynchronized episodes lasting for one cycle of oscillations to the relative frequency of desynchronized episodes longer than four cycles (similar to how it was used in experimental studies by Ahn et al., 2014, 2018 and Malaia et al., 2020). Thus, a larger value of desynchronization ratio points to a larger number of short desynchronizations.

III. RESULTS

In each network, we choose an excitatory neuron that has a higher firing rate and study the synchronized dynamics between them (although, to reflect the network dynamics, we report the average firing frequency in the network; both faster and slower neurons' frequencies are close to each other). With weak to moderate connections between circuits, the network exhibits partially synchronized activity [see Fig. 1(c) for time-series for an example of voltage and raster plots of spiking in all neurons]. This section presents the results of numerical simulations of how synaptic excitation and

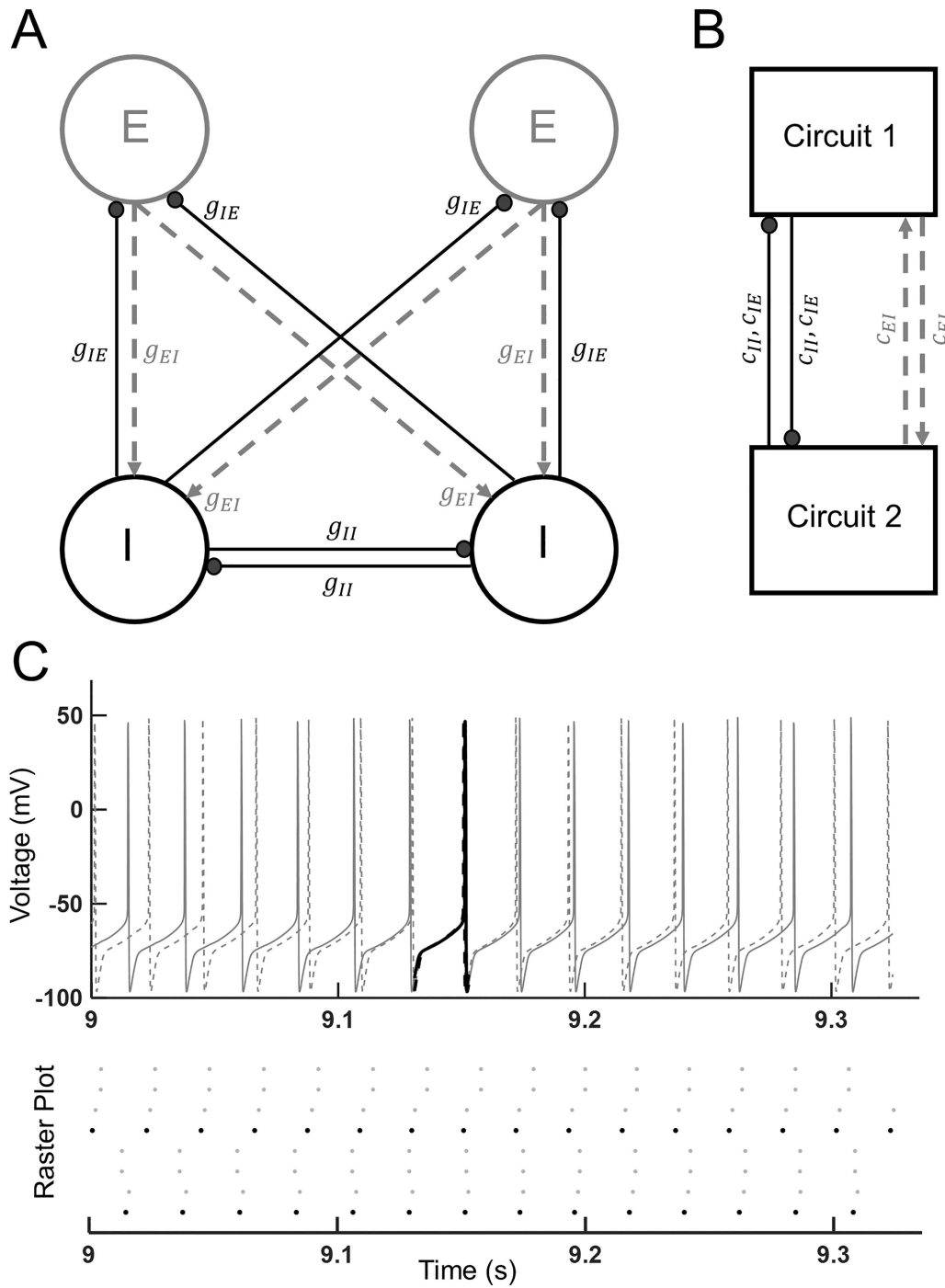


FIG. 1. Schematic of the model circuitry. (a) An individual circuit consists of two excitatory and two inhibitory neurons with excitatory connections g_{EI} (dashed gray with an arrow at the end) and inhibitory connections g_{II} and g_{IE} (solid black with a circle at the end). (b) Full model circuitry has two individual circuits. Two circuits are connected by inhibitory synapses c_{IE} and c_{II} (solid black) and excitatory synapses c_{EI} (dotted gray). There are no mutual connections between excitatory neurons. (c) Voltage traces of an excitatory neuron from two circuits (gray and black lines) and the raster plot of all the neurons in both networks. The two excitatory neurons with voltage traces above are in black, and the rest of the neurons are in gray.

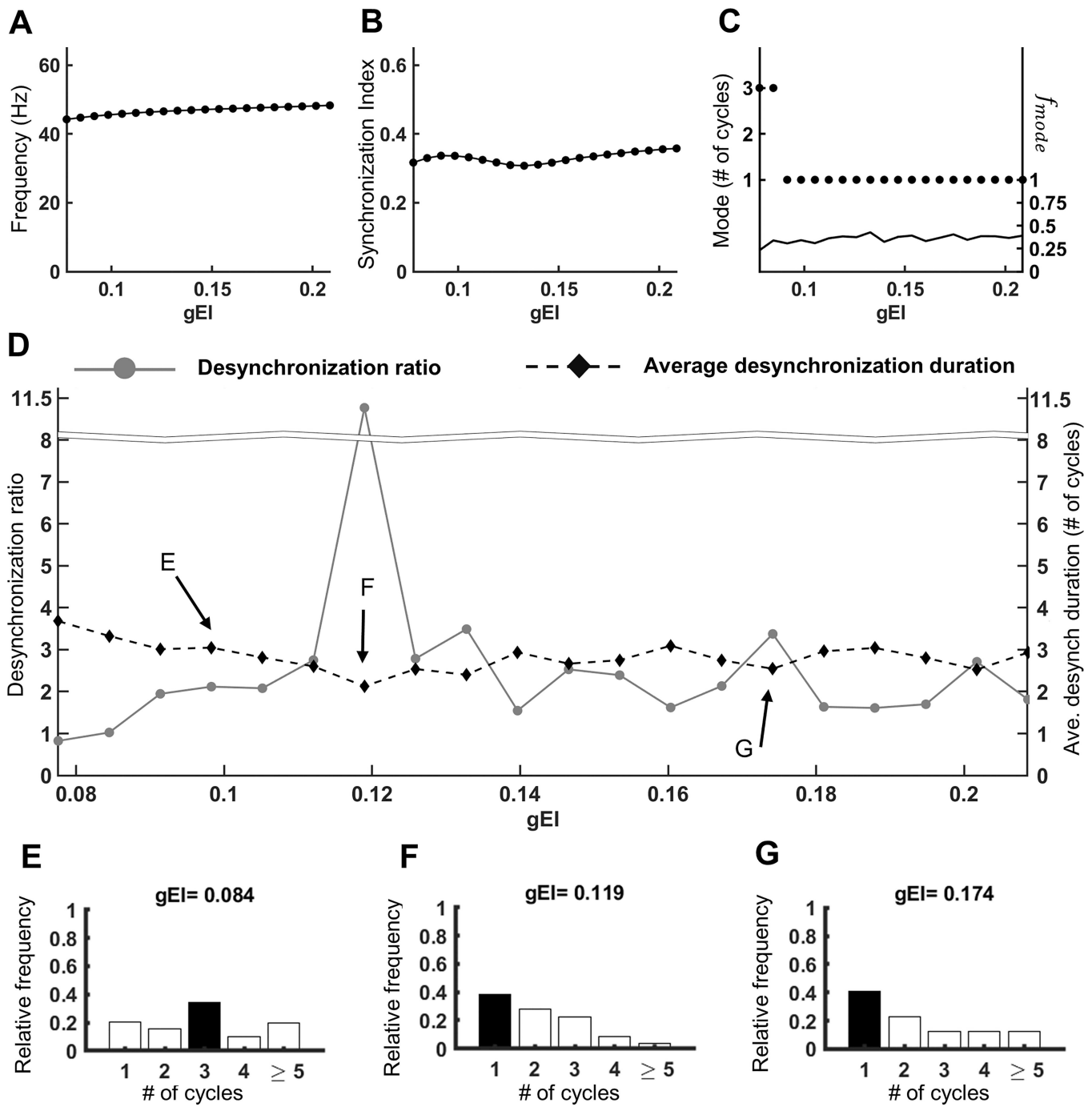


FIG. 2. Effect of within-circuit excitatory to inhibitory neuron synaptic connection g_{EI} on the temporal patterning of synchronized dynamics. (a) Average firing frequency in Hz. (b) Synchronization index. (c) The mode (number of cycles) of the desynchronization duration distribution (black dots) and the frequency of the mode f_{mode} (black curve). (d) Average desynchronization duration (number of cycles) in a dashed black line with diamonds and the desynchronization ratio in a solid gray line with circles. Examples of the distribution of desynchronization durations are shown in panels E–G; the horizontal axis is the duration of desynchronizations as measured in the cycles of oscillations. The mode of the desynchronization distribution is highlighted as a black bar in each histogram. The arrows in panel D indicate the cases that correspond to the histograms shown in panels E–G.

inhibition and kinetics of ionic channels affect the temporal patterning of this partially synchronized neural oscillations.

A. Synaptic effects on the temporal pattern of synchronization

1. The effect of excitation

We consider variation of both within-circuit excitatory connections g_{EI} and cross-circuit excitatory connections c_{EI} . We vary g_{EI} from 0.08 to 0.21. In this range, the average firing frequency of the network stays in the 44–48 Hz range [Fig. 2(a)]. The synchronization index is in the 0.3–0.36 range [Fig. 2(b)]. There is a pronounced change in the mode of the distribution of the desynchronization durations; it changes from 3 to 1 as synaptic strength g_{EI} increases [Fig. 2(c)]. Mode 1 is observed in a relatively large range of g_{EI} (and is typical for various experimental observations). The average desynchronization duration is generally decreasing from about four cycles to about two cycles [Fig. 2(d)]. The desynchronization ratio (see Sec. II) shows substantial variation. It increases from about 1 to about 3 with one isolated case of almost 12 (driven by a very small value of the relative frequency of long desynchronizations) and then it fluctuates in between 2 and 4 [Fig. 2(d)]. We would like to note that a very high value of desynchronization ratio may not necessarily carry a high precision; nevertheless, it points to the fact that long desynchronizations are really rare.

Panels E–G show examples of distributions of desynchronization durations for three different values of g_{EI} . Example E shows desynchronization distribution with mode 3; the average desynchronization duration is relatively large, and the desynchronization ratio is relatively small. Examples F and G show a desynchronization duration distribution with mode 1. While F and G have the same mode, example F has a much higher value of a desynchronization ratio because it has a much smaller number of long desynchronizations (lasting 5 and more cycles). The average values of desynchronization durations in both cases are roughly similar. Nevertheless, these examples show a general trend of desynchronizations becoming shorter. These examples corroborate the weak trend described in the previous paragraph: as we increase excitatory synapse strength g_{EI} , the desynchronizations become progressively shorter.

Note that mode and average (mean) may have substantially different values. This is probably not surprising (especially given that experimental studies report the mode equal to one; therefore, the average must be larger). It is not clear which particular characteristic of the distribution is of a most biological importance; therefore, mode, desynchronization ratio (as reported in experiments cited in Sec. I), and the average value are presented to better illustrate the dynamics.

Next, we examine the effect of cross-circuit excitatory to inhibitory connection c_{EI} by varying its value from 0 to 0.04. The average firing rate mildly increases from 45 to 47 Hz [Fig. 3(a)], while the synchronization index stays within the 0.3–0.35 range [Fig. 3(b)]. The distribution of desynchronization duration shows substantial changes with different values of c_{EI} ; see Fig. 3(c). For smaller values of c_{EI} , the mode of the distribution is mostly 1. However, for larger values of c_{EI} , the desynchronization duration distribution has predominantly mode 3 (although mode 1 and 2 are also present).

Figure 3(d) shows how the desynchronization ratio and the average desynchronization duration are changing with c_{EI} . They vary around 2 and 3, respectively, in the c_{EI} range that produces mostly distributions with mode 1. However, the distribution shows more prominent changes as can be seen in panels E–G: smaller values of c_{EI} (example E) yield a sharper and more prominent mode 1 (more similar to those observed in experiments) than larger values of c_{EI} (example F). Example G exhibits distribution with mode 3. Note that even though the desynchronization ratio is high for the distribution in G, the mode is not 1. Thus, as we mentioned above, the desynchronization ratio alone is not sufficient to distinguish between short and long desynchronization dynamics.

2. The effect of inhibition

There are two kinds of inhibitory connections in the model: inhibitory to excitatory neurons and inhibitory to inhibitory neuron connections. We examine the impact of both kinds of inhibitory connections on the temporal patterning of synchronization, looking at within-circuit connections (g_{IE} and g_{II}) as well as cross-circuit connections (c_{IE} and c_{II}).

Local inhibitory to excitatory connection g_{IE} is varied from 0.6 to 1.36. Within this range, the average frequency decreases significantly from 49 to 36 Hz [Fig. 4(a)]. This is expected; larger g_{IE} results in more inhibition input for excitatory cells and thus reduces the firing rate. The synchronization index varies from 0.3 to about 0.43 [Fig. 4(b)]. The mode of the desynchronization duration distribution is mostly 1 [Fig. 4(c)]. There is only one isolated case in which desynchronization duration has a higher mode. Furthermore, as g_{IE} increases, the desynch ratio (although variable) shows a generally increasing trend and almost triples from 2 to 6; see Fig. 4(d). The average desynchronization duration mildly varies between 2 and 3; see Fig. 4(d). Examples of the desynchronization duration distribution are shown in panels E–G. Example E shows a histogram for the case of a small g_{IE} value. While the mode is 1, the likelihood of a desynchronization duration lasting one cycle is similar to the likelihood of longer durations. Thus, the desynchronization ratio is low. Examples F and G illustrate histograms for the cases of larger g_{IE} values, and the mode (which is 1) is more prominent in both cases. While desynchronization distributions in F and G have similar average durations, the desynchronization ratio in G is noticeably bigger. Thus, in general, larger values of g_{IE} tend to promote shorter desynchronization.

Similarly, we examine the effect of cross-circuit inhibitory to excitatory connection c_{IE} . When c_{IE} goes from 0 to 0.08, the average firing rate decreases from 47 to 41 Hz [Fig. 5(a)], and the synchronization index shows a mild increase from 0.31 to 0.37 [Fig. 5(b)]. The mode of desynchronization durations is mostly 1, and there are a couple isolated cases of mode 2 [Fig. 5(c)]. Furthermore, the average mode increases, and the desynchronization ratio decreases [Fig. 5(d)]. Thus, the desynchronizations have a weak tendency of becoming longer as the cross-circuit inhibitory coupling goes up. Examples in panels F and G both show the distribution with mode 1; however, mode 1 in example F is more prominent than mode 1 in example G.

Within-circuit inhibitory to inhibitory connection g_{II} is varied from 0.14 to 1. The average frequency varies minimally in

between 44 and 46.5 Hz; see Fig. 6(a). The synchronization index first increases and then decreases but stays in between 0.29 and 0.33; see Fig. 6(b). The desynchronization duration distribution shows some substantial variations; see Fig. 6(c). The higher mode cases all occur for higher values of g_{II} . The desynchronization ratio decreases sharply from 12 to 2, and then it stays around 1 to 2; the average desynchronization duration increases slowly from 2 to 4; see Fig. 6(d). The example in panel E portrays the distribution with a prominent mode 1 and a small probability of any duration lasting five cycles or more; thus, the desynchronization ratio is large. Examples F and G show distributions for larger values g_{II} . In this region, the distribution can either have a higher mode (mode 3 in example F) or a lower mode 1 (example G). Either way, the distribution is flatter, and thus, larger values of g_{II} tend to produce longer desynchronization durations.

Between-circuit inhibitory to inhibitory connection c_{II} is varied from 0 to 0.11. The average frequency decreases from 46 to 43 Hz; see Fig. 7(a). The synchronization index varies in the range of 0.32 and 0.26; see Fig. 7(b). The distribution of desynchronization durations has mode 1 in all cases; see Fig. 7(c). The average values of desynchronization durations appear to have a very weak decreasing trend, while the desynchronization ratio has a weak increasing trend; see Fig. 7(d). Panels E–G portray examples of desynchronization duration distributions for small and large values of c_{II} . In the first example E, the probability of desynch duration lasting one cycle is close to the probability of longer cycles. In panels F and G, the likelihood of desynchronization duration lasting one cycle is larger than that of longer durations. Also, mode 1 in panel G is more prominent than mode 1 in panel F. Overall, larger c_{II} shows a weak tendency for shorter desynchronizations.

3. Changes in the desynchronization durations can be independent of the frequency and of the average synchronization strength

In Secs. III A 1 and III A 2, we see that changes in the desynchronization durations are often accompanied by the changes in the frequency of oscillations and the average synchronization strength. Here, we consider situations, where synchrony and frequency are not changing, while desynchronization durations are. We would like to note that since the time-series analysis method used here measures desynchronization durations in relative units (cycles of oscillations), it is interesting to see what happens when the frequency is fixed (otherwise, changes in the desynchronization durations as measured in cycles may not necessarily translate into the same changes in desynchronization duration measured in the absolute time units). To keep frequency and synchronization index relatively constant, yet to alter the temporal pattern of synchrony, we co-vary multiple synaptic strengths. Specifically, we increase within-circuit connections (g_{IE} and g_{EI}) and decrease between-circuit connections (c_{IE} and c_{EI}) at the same time, parameterizing all of them as a linear function of parameter k ,

$$g_{EI} = 0.0012k + 0.096 \quad g_{IE} = 0.0041k \\ + 0.8205 \text{ for } k = 1, 2, \dots, 31, \quad (12)$$

$$c_{EI} = -0.0004k + 0.038 \quad c_{IE} = -0.0008k \\ + 0.076 \text{ for } k = 1, 2, \dots, 31. \quad (13)$$

Within this range of parameters, the average frequency is relatively constant around 40 Hz [Fig. 8(a)]; the synchronization index is near 0.37 and does not show substantial variation either [Fig. 8(b)]. When k is small (weak local connections and strong cross-circuit connections), the desynchronization duration distribution has mode equal to 3 [Fig. 8(c)]. When k is larger (strong local connections and weak cross-circuit connections), the desynchronization duration distribution has mode equal to 1 [Fig. 8(c)]. The average desynchronization duration goes down, while the desynchronization ratio shows a prominent increase, pointing to desynchronizations getting shorter [Fig. 8(d)]. This trend is further illustrated in panels E–G with examples of desynchronization duration distributions. Example E has mode 3. Examples F and G have mode 1, and mode 1 is more prominent in example G than in example F. We see that the temporal patterning of synchronized activity may show very substantial changes, while average synchrony and frequency are relatively constant. In other words, average synchronization and temporal patterning can be independent of each other.

B. The effect of membrane current kinetics on the temporal pattern of synchronization

An earlier modeling study in a simple network of two mutually excitatory coupled simplified Hodgkin–Huxley-like model neurons (Ahn and Rubchinsky, 2017) showed that temporal patterning of synchronization is sensitive to the parameters defining the time scale of the delayed-rectifier potassium current (responsible for a relaxational character of spiking oscillations in that model). Hence, we want to explore if the model used here (a more complicated network structure with excitation and inhibition and more adequate models of individual neurons) shows a similar dependence of desynchronization durations on the membrane current kinetics.

Similar to Ahn and Rubchinsky (2017), we will look at the effect of the peak value of the voltage-dependent activation time constant and the width of voltage-dependence of the activation time constant of potassium current (both parameters effectively make this current faster or slower to activate, either directly or indirectly) on the temporal patterning of synchronization. The activation time constant of the potassium channel is given by

$$\tau_n(V) = \frac{1}{\alpha_n(V) + \beta_n(V)}, \quad (14)$$

where $\alpha_n(V)$ and $\beta_n(V)$ are the opening and closing function of the potassium channel [see Eqs. (6) and (9) in Sec. II]. We parameterize $\alpha_n(V)$ and $\beta_n(V)$ as follows:

$$\alpha_n(V) = \frac{\varepsilon \alpha_1(V+52)}{1 - \exp\left(-\frac{V+52}{\delta \alpha_2}\right)} \quad \beta_n(V) = \varepsilon \beta_1 \exp\left(-\frac{V+57}{\delta \beta_2}\right). \quad (15)$$

Here, $\alpha_1, \alpha_2, \beta_1, \beta_2$ are default values of the opening and closing functions (see Sec. II). Provided that everything else is fixed, varying parameter ε leads to change of the amplitude of the activation time constant $\tau_n(V)$. Larger values of ε lead to faster activation of potassium delayed-rectifier current and thus a less spiky (closer to a sinusoidal waveform) profile of voltage. On the other hand,

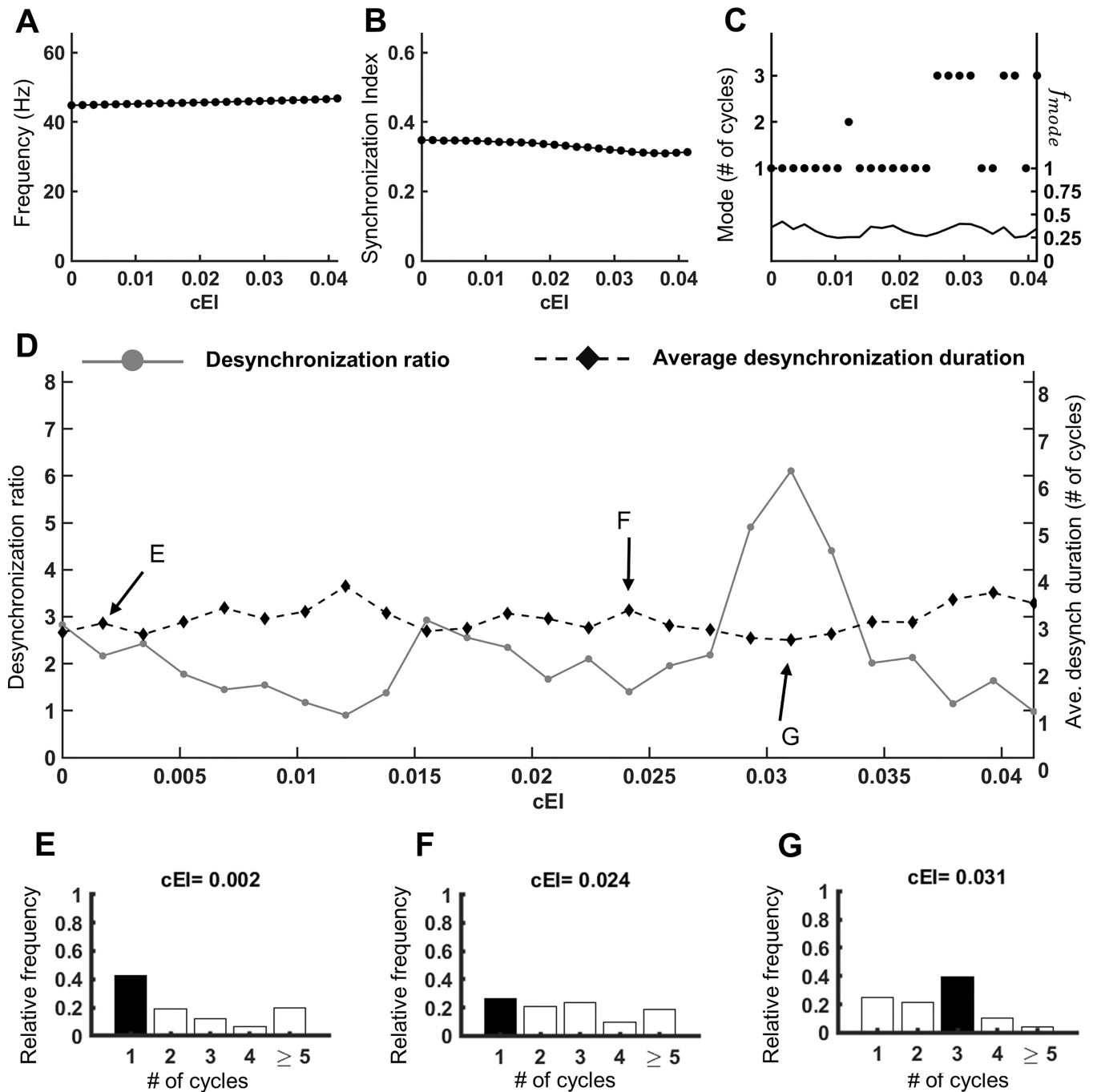


FIG. 3. Effect of between-circuit excitatory to inhibitory neuron synaptic connection c_{EI} on the temporal patterning of synchronized dynamics. (a) Average firing frequency in Hz. (b) Synchronization index. (c) The mode (number of cycles) of the desynchronization duration distribution (black dots) and the frequency of the mode f_{mode} (black curve). (d) Average desynchronization duration (number of cycles) in a dashed black line with diamonds and a desynchronization ratio in a solid gray line with circles. Examples of the distribution of desynchronization durations are shown in panels E–G; the horizontal axis is the duration of desynchronizations as measured in the cycles of oscillations. The mode of the desynchronization distribution is highlighted as a black bar in each histogram. The arrows in panel D indicate the cases that correspond to the histograms shown in panels E–G.

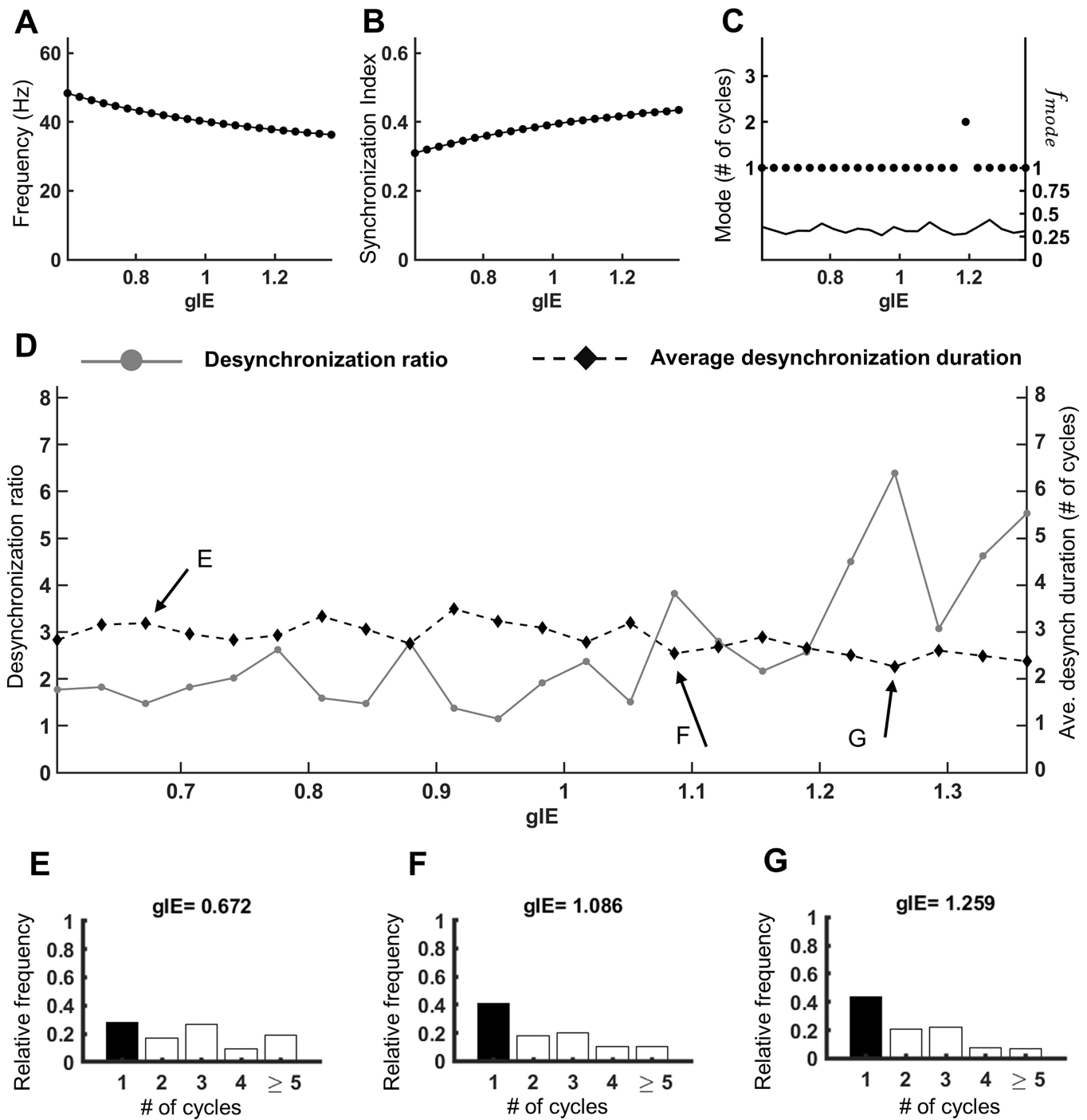


FIG. 4. Effect of within-circuit inhibitory to excitatory neuron synaptic connection g_{IE} on the temporal patterning of synchronized dynamics. (a) Average firing frequency in Hz. (b) Synchronization index. (c) The mode (number of cycles) of the desynchronization duration distribution (black dots) and the frequency of the mode f_{mode} (black curve). (d) Average desynchronization duration (number of cycles) in a dashed black line with diamonds and the desynchronization ratio in a solid gray line with circles. Examples of the distribution of desynchronization durations are shown in panels E–G; the horizontal axis is the duration of desynchronizations as measured in the cycles of oscillations. The mode of the desynchronization distribution is highlighted as a black bar in each histogram. The arrows in panel D indicate the cases that correspond to the histograms shown in panels E–G.

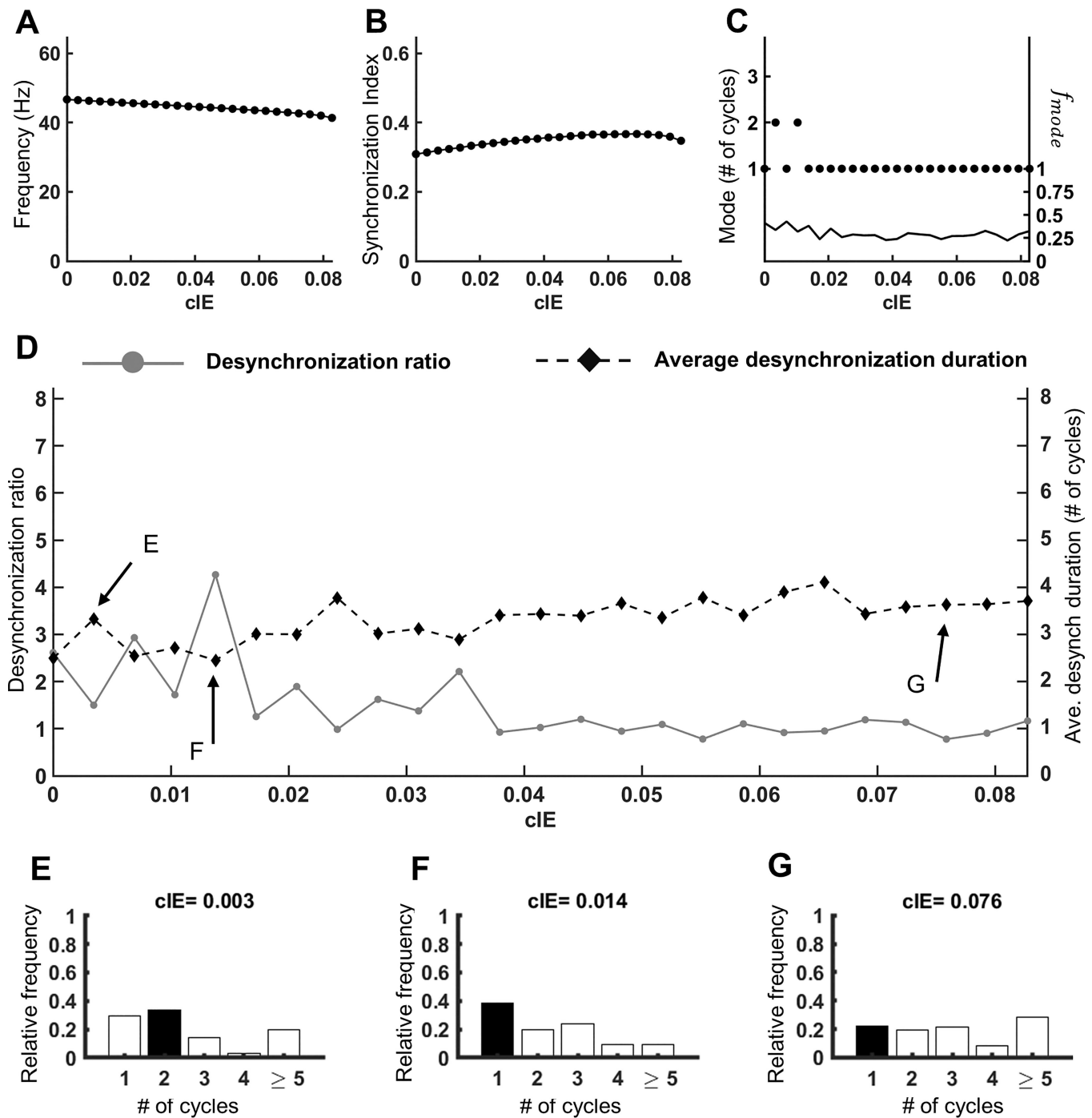


FIG. 5. Effect of between-circuit inhibitory to excitatory neuron synaptic connection c_{IE} on the temporal patterning of synchronized dynamics. (a) Average firing frequency in Hz. (b) Synchronization index. (c) The mode (number of cycles) of the desynchronization duration distribution (black dots) and the frequency of the mode f_{mode} (black curve). (d) Average desynchronization duration (number of cycles) in a dashed black line with diamonds and the desynchronization ratio in a solid gray line with circles. Examples of the distribution of desynchronization durations are shown in panels E–G; the horizontal axis is the duration of desynchronizations as measured in the cycles of oscillations. The mode of the desynchronization distribution is highlighted as a black bar in each histogram. The arrows in panel D indicate the cases that correspond to the histograms shown in panels E–G.

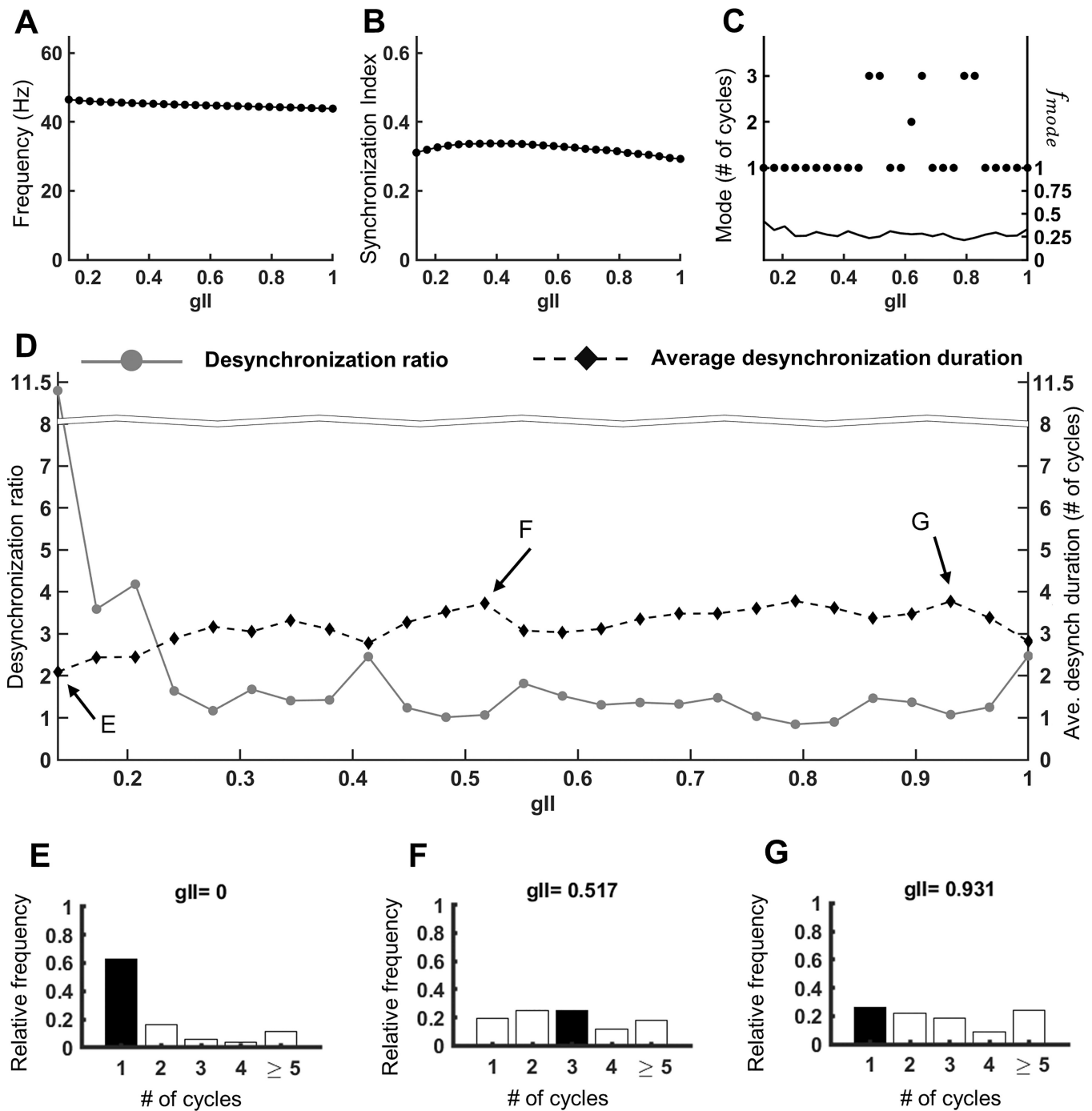


FIG. 6. Effect of within-circuit inhibitory to inhibitory neuron synaptic connection g_{II} on the temporal patterning of synchronized dynamics. (a) Average firing frequency in Hz. (b) Synchronization index. (c) The mode (number of cycles) of the desynchronization duration distribution (black dots) and the frequency of the mode f_{mode} (black curve). (d) Average desynchronization duration (number of cycles) in a dashed black line with diamonds and a desynchronization ratio in a solid gray line with circles. Examples of distribution of desynchronization durations are shown in panels E–G; the horizontal axis is the duration of desynchronizations as measured in the cycles of oscillations. The mode of the desynchronization distribution is highlighted as a black bar in each histogram. The arrows in panel D indicate the cases that correspond to the histograms shown in panels E–G.

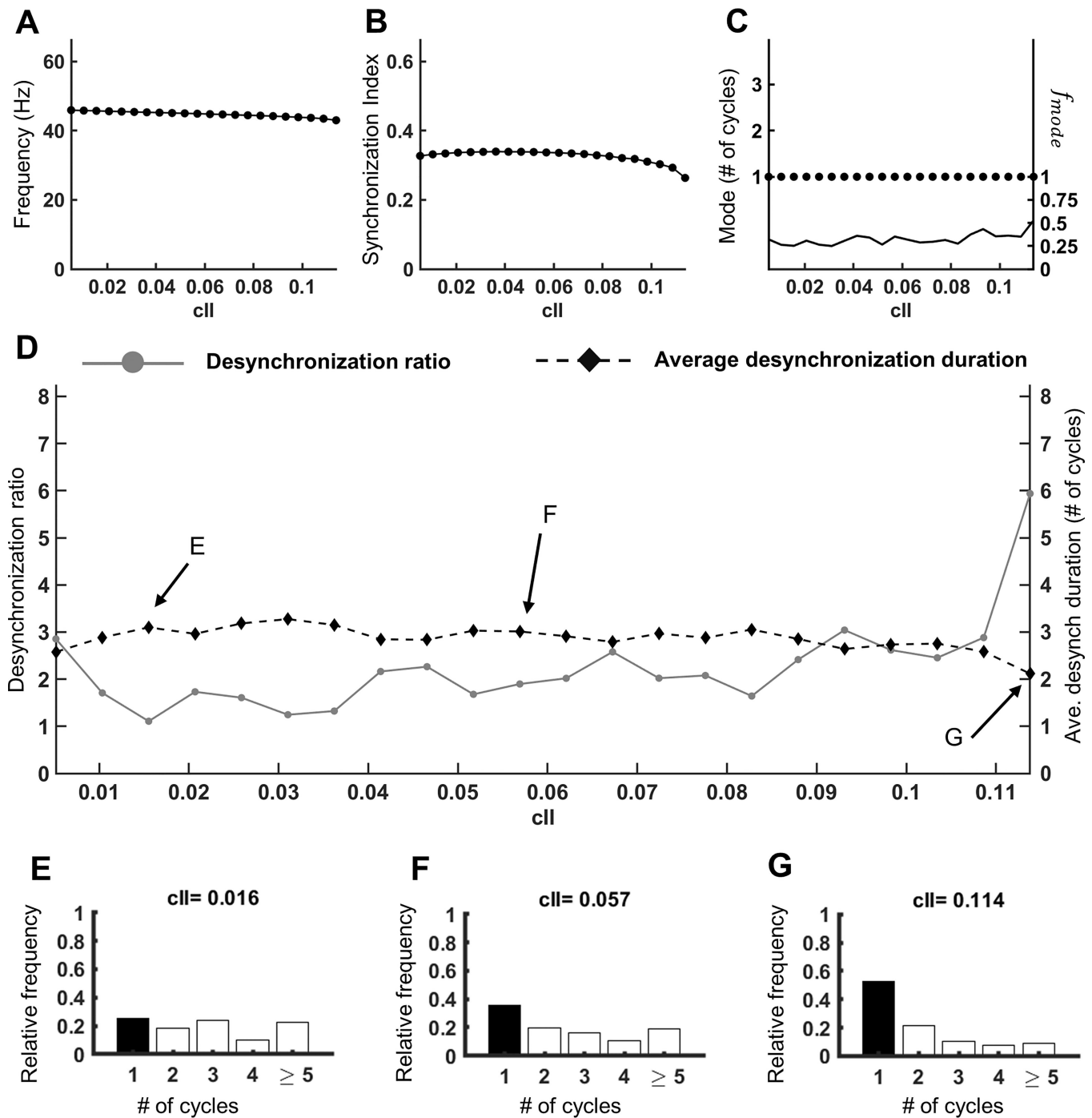


FIG. 7. Effect of between-circuit inhibitory to inhibitory neuron synaptic connection c_{II} on the temporal patterning of synchronized dynamics. (a) Average firing frequency in Hz. (b) Synchronization index. (c) The mode (number of cycles) of the desynchronization duration distribution (black dots) and the frequency of the mode f_{mode} (black curve). (d) Average desynchronization duration (number of cycles) in a dashed black line with diamonds and a desynchronization ratio in a solid gray line with circles. Examples of the distribution of desynchronization durations are shown in panels E–G; the horizontal axis is the duration of desynchronizations as measured in the cycles of oscillations. The mode of the desynchronization distribution is highlighted as a black bar in each histogram. The arrows in panel D indicate the cases that correspond to the histograms shown in panels E–G.

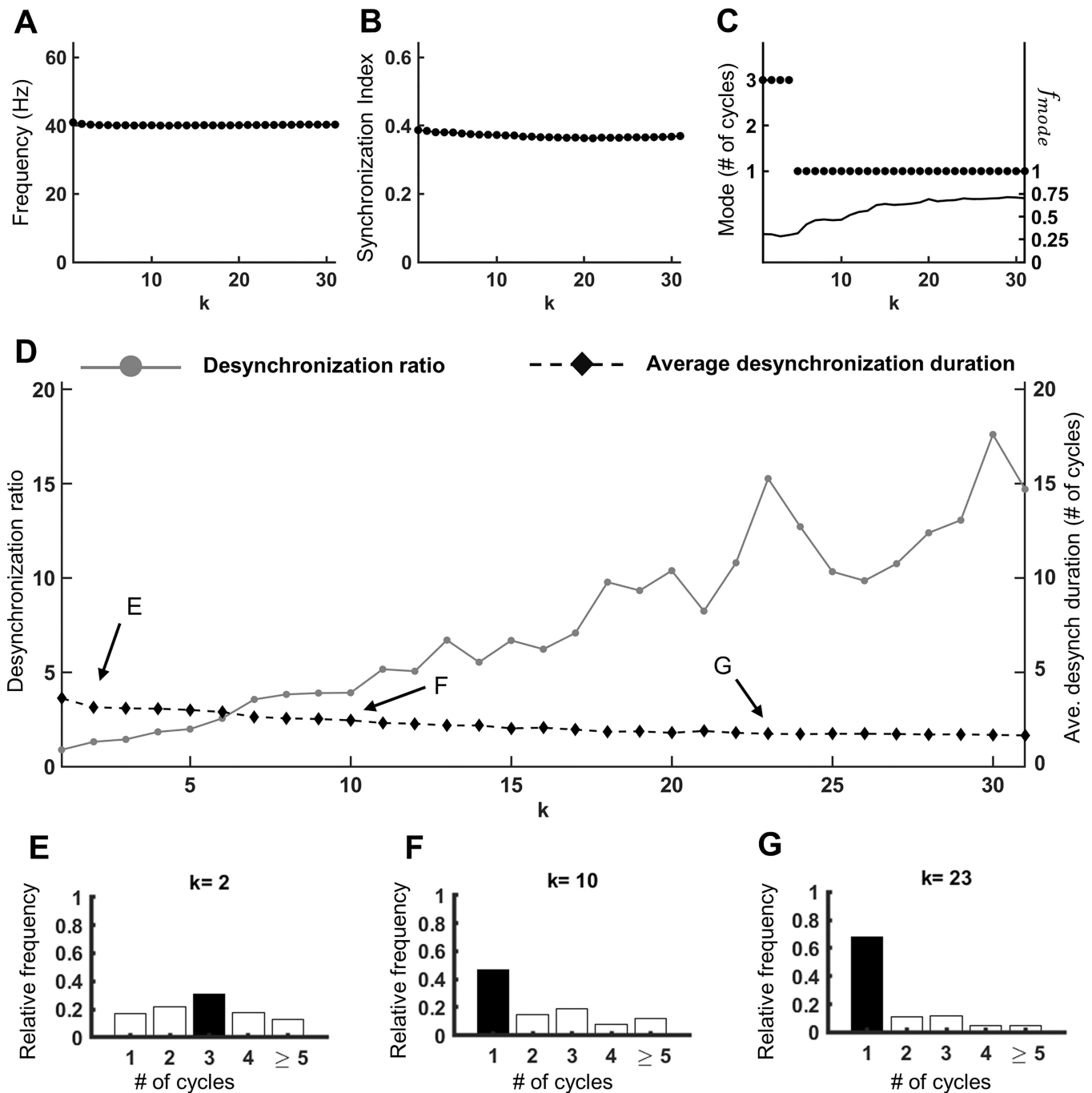


FIG. 8. Changes in the desynchronization durations can be independent of the frequency and of the average synchronization strength. Local connections between excitatory and inhibitory units g_{IE} and g_{EI} are increased, while cross-circuit connections between excitatory and inhibitory cells c_{IE} and c_{EI} are decreased as linear functions of k ; see Eqs. (12) and (13). (a) Average firing frequency in Hz. (b) Synchronization index. (c) The mode (number of cycles) of the desynchronization duration distribution (black dots) and the frequency of the mode f_{mode} (black curve). (d) Average desynchronization duration (number of cycles) in a dashed black line with diamonds and a desynchronization ratio in a solid gray line with circles. Examples of the distribution of desynchronization durations are shown in panels E–G; the horizontal axis is the duration of desynchronizations as measured in the cycles of oscillations. The mode of the desynchronization distribution is highlighted as a black bar in each histogram. The arrows in panel D indicate the cases that correspond to the histograms shown in panels E–G.

changing parameter δ results in change of the width of the activation time constant $\tau_n(V)$. Larger values of δ also lead to a sinusoidal waveform of voltage trace.

The value of ε is varied from 0.4 to 3 for all neurons in both circuits. Naturally, this change of the time scale affects the firing rate of the neurons (it moves up from 42 to 51 Hz); see Fig. 9(a). The synchronization index stays in the range of 0.3–0.35; see Fig. 9(b). The shape of the spike is affected too). When ε is small, the mode of the desynch distribution is 1. For larger values of ε , the mode of the desynchronization duration distribution may be 2 or 3; if the mode is 1 in this region, it is not as prominent as mode 1 from small values of ε [Fig. 9(c)]. The average desynchronization duration is increasing, while the desynchronization ratio is decreasing as ε becomes bigger [Fig. 9(d)]. Examples of the desynchronization duration distributions (shown in panels E–G) illustrate this trend. Thus, slow activation of potassium current (as in the original model, i.e., physiologically realistic and slower) leads to dynamics with shorter desynchronizations. This is consistent with the prior study (Ahn and Rubchinsky, 2017).

The value of δ is varied between 0.4 and 1.25 for all neurons in both circuits. The average frequency is barely affected by this change, staying in between 45 and 46 Hz [Fig. 10(a)]. The synchronization index decreases from 0.47 to 0.33 [Fig. 10(b)]. While the mode of the desynchronization duration distribution is always 1, the prominence of the mode consistently decreases [Fig. 10(c)]. Fitting the same trend, the average desynchronization duration decreases, and the desynchronization ratio increases [Fig. 10(d)]. Three examples of desynchronization duration distributions shown in panels E–G further illustrate this. Mode 1 is more prominent when δ is small (example E) as compared to when δ is large (examples F and G). The distribution in panel G has a smaller mode 1 than the distribution in panel F. Thus, smaller δ and resulting slower activation of the delayed-rectifier potassium current produce shorter desynchronizations. This is also in agreement with the prior study (Ahn and Rubchinsky, 2017).

IV. DISCUSSION

A. Summary and significance of findings: Connectivity strength affects temporal patterning of network synchronization

We studied the properties of synchronized dynamics of a neural network consisting of two circuits exhibiting the PING gamma rhythm. For moderate connectivity strength, gamma oscillations are only partially synchronized, and thus, the intervals of highly synchronous activity are interspersed with intervals of low synchrony activity. We found that the temporal patterning of this synchronized activity depends on the strength of connections in the network. Thus, changing synaptic strength affects the distribution of desynchronization event duration (affects the relative duration of the intervals during which the activity is not synchronized).

More specifically, local connections and cross-circuit connections have opposite effects on the temporal pattern of synchronization/desynchronization. Stronger local connections between inhibitory and excitatory neurons (both E–I and I–E synapses within circuits) and weaker cross-circuit connections between inhibitory

and excitatory neurons (both E–I and I–E synapses between circuits) promote dynamics with predominantly short desynchronizations. These trends are observed for both independent and simultaneous variation of these synapses. The situation is inverted for connections between inhibitory interneurons. Weaker local connections between inhibitory cells (I–I connections within circuits) and stronger cross-circuit connections between inhibitory cells (I–I connections between circuits) promote dynamics with predominantly short desynchronizations.

We also considered the effect of membrane current kinetics on the temporal patterning of synchronization. While the current kinetics may be harder to change in the experiment than synaptic strength, prior modeling studies with minimal neural circuits indicated that it may affect the fine temporal structure of neural synchronization (Ahn and Rubchinsky, 2017). We found that different ways of slowing the kinetics of delayed-rectifier potassium current (which make a neuron a more relaxational oscillator and lead to a more spiky profile of neural voltage) facilitate short desynchronizations.

Furthermore, we showed that the temporal pattern of synchronization can vary independently of the average synchronization strength. At the same time, the firing frequency can be kept almost constant so that changes of the desynchronization durations are apparent not only in relative time units (cycles of oscillations) but also in absolute time units (milliseconds). Thus, even though average synchronization strength and the temporal pattern of synchrony can co-vary together, they can also vary independently of each other and are independent characteristics of synchronized phenomena in neural networks.

B. Computational results in the context of experimental studies: Prevalence of short desynchronization dynamics and the role of synaptic coupling

Even though the distribution of durations of desynchronization events was found to depend on the properties of neurons and synapses, a review of all the numerical results of this study suggests that partially synchronized dynamics in the PING gamma network has predominantly short desynchronizations. These short desynchronized intervals may be numerous so that the average synchrony level may be low. This is not necessarily true for a generic oscillatory network; the same level of synchrony may be reached with many short desynchronizations and a few long desynchronizations (Ahn *et al.*, 2011 and Ahn and Rubchinsky, 2017).

However, in the realistic (in the dynamics of neurons and synapses) network studied here, there is a tendency for short desynchronization dynamics. Importantly, the application of the same time-series analysis techniques as used here to various recordings of the electric activity of the brain indicates that it is essentially always dominated by short desynchronizations regardless of the brain area, type of recording, disease status, and brain rhythm. This was observed in the beta band spiking units, local field potential (LFP), and EEG in Parkinson's disease and its animal model in the basal ganglia and motor cortex (Park *et al.*, 2010; Ratnadurai-Giridharan *et al.*, 2016; Ahn *et al.*, 2018; and Dos Santos Lima *et al.*, 2020), alpha and beta bands in EEG in healthy subjects

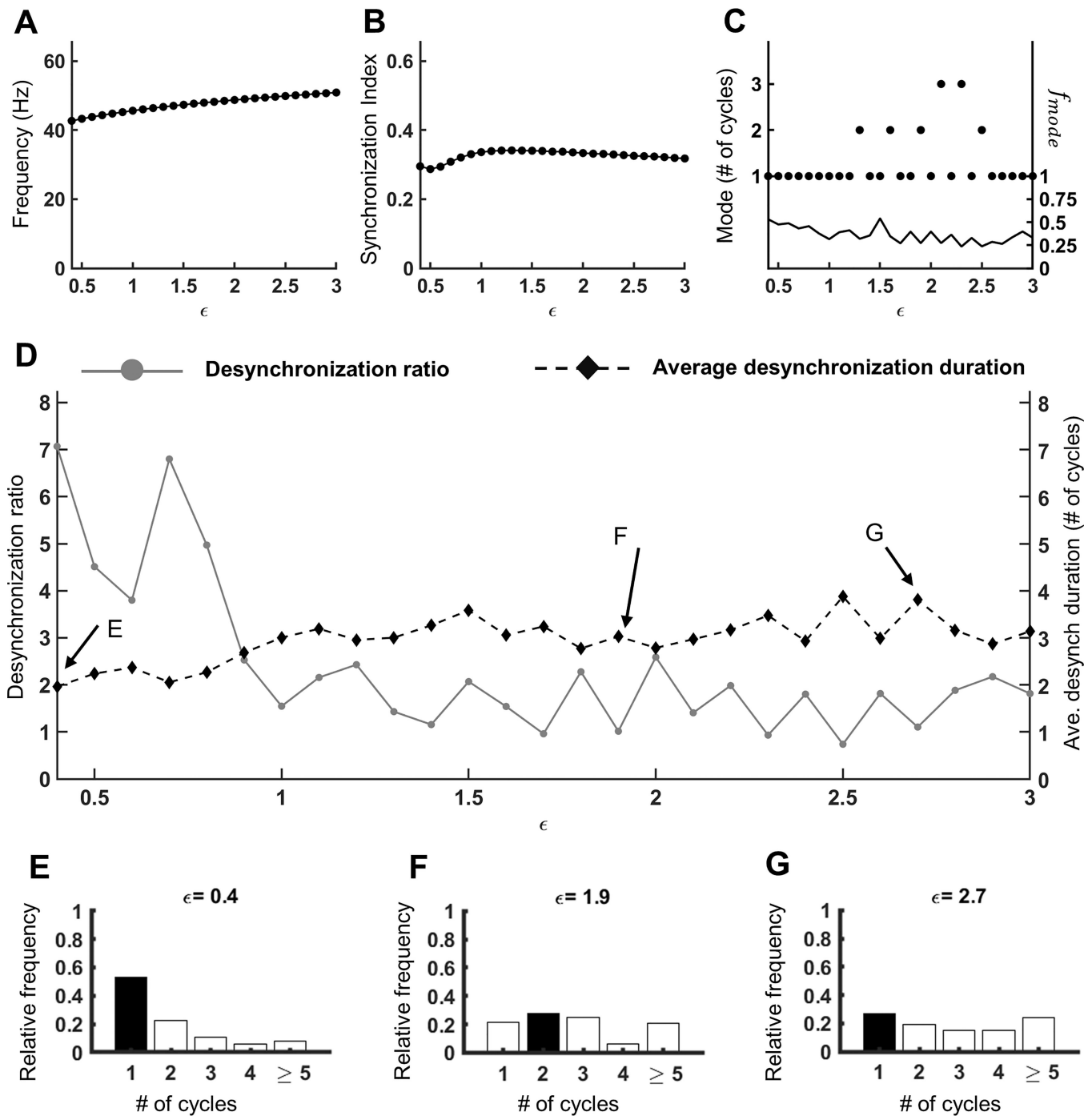


FIG. 9. Effect of the peak value of the activation time constant of the potassium channel on the temporal patterning of synchronized dynamics. The peak value of the activation time constant is written as a function of ϵ ; see Eqs. (14) and (15). (a) Average firing frequency in Hz. (b) Synchronization index. (c) The mode (number of cycles) of the desynchronization duration distribution (black dots) and the frequency of the mode f_{mode} (black curve). (d) Average desynchronization duration (number of cycles) in a dashed black line with diamonds and a desynchronization ratio in a solid gray line with circles. Examples of the distribution of desynchronization durations are shown in panels E–G; the horizontal axis is the duration of desynchronizations as measured in the cycles of oscillations. The mode of the desynchronization distribution is highlighted as a black bar in each histogram. The arrows in panel D indicate the cases that correspond to the histograms shown in panels E–G.

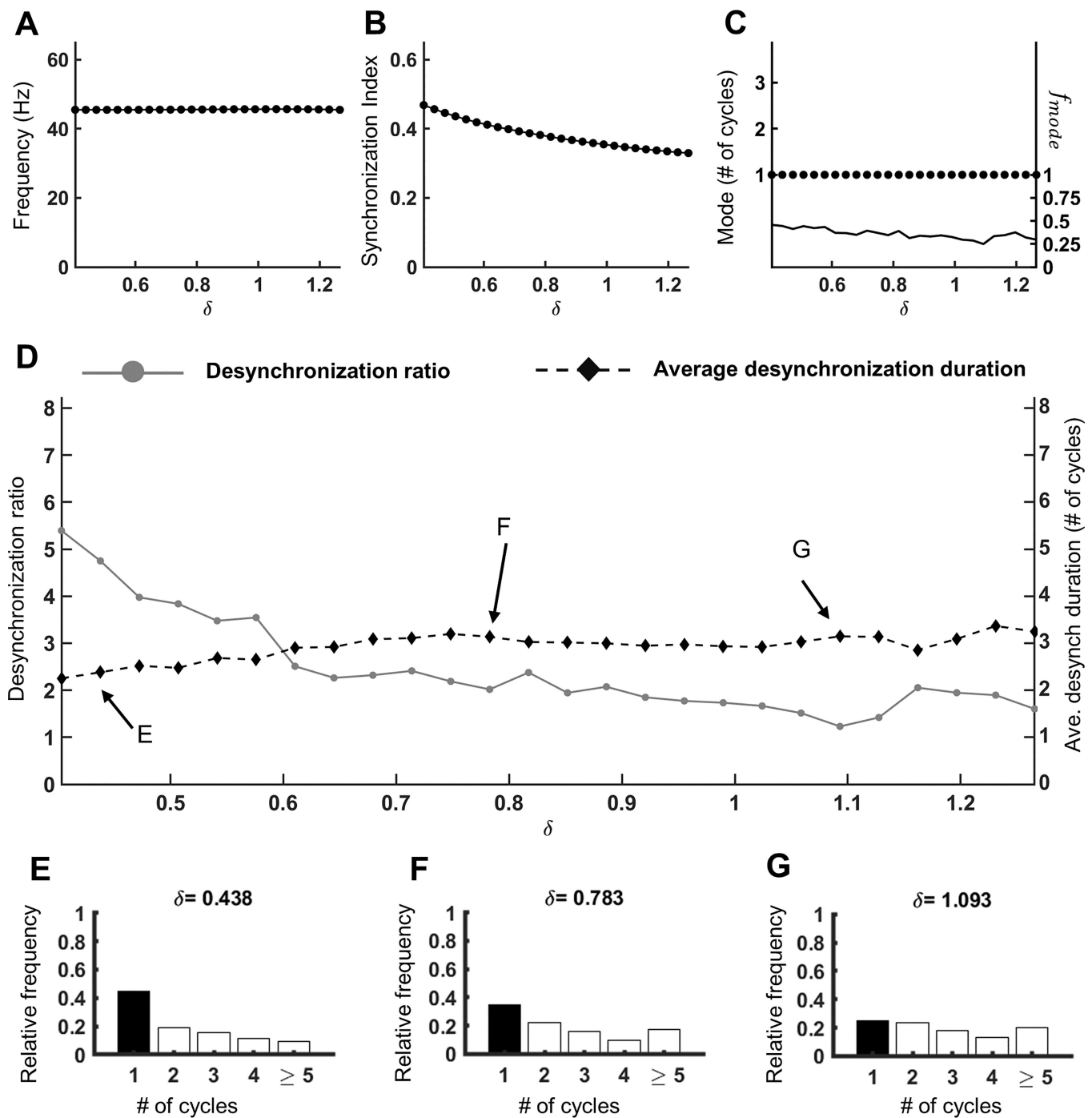


FIG. 10. Effect of the width of voltage-dependence of the activation time constant of the potassium channel on the temporal patterning of synchronized dynamics. The width of voltage-dependence of the activation time constant is parameterized by δ ; see Eqs. (14) and (15). (a) Average firing frequency in Hz. (b) Synchronization index. (c) The mode (number of cycles) of the desynchronization duration distribution (black dots) and the frequency of the mode f_{mode} (black curve). (d) Average desynchronization duration (number of cycles) in a dashed black line with diamonds and a desynchronization ratio in a solid gray line with circles. Examples of the distribution of desynchronization durations are shown in panels E–G; the horizontal axis is the duration of desynchronizations as measured in the cycles of oscillations. The mode of the desynchronization distribution is highlighted as a black bar in each histogram. The arrows in panel D indicate the cases that correspond to the histograms shown in panels E–G.

(Ahn and Rubchinsky, 2013), the theta band in prefrontal cortex and hippocampus in normal and drug-sensitized rodents (Ahn *et al.*, 2014), and theta, beta, and low frequency gamma in EEG in subjects with and without autism spectrum disorder (Malaia *et al.*, 2020). The results of the present study provide an additional support for the hypothesis that short desynchronizations dynamics may be common in the synchronization of the oscillations of the neural activity of the brain.

The experimental studies discussed above also found that the changes in the temporal pattern of neural synchrony may be related to behavioral changes, and this may be true even if the average synchronization strength is not changed (Ahn *et al.*, 2014; 2018 and Malaia *et al.*, 2020). Even though most of these studies did not consider gamma rhythm, what we found out in the present study of neural networks with PING gamma may fit with this general framework of importance of the fine temporal structure of synchronized dynamics. We found that the synchrony pattern may vary if the synaptic strength is varied (and it may vary independently of the synchronization strength). PING gamma is known to depend on the synaptic strength of different types of synapses involved (e.g., Buzsáki and Wang, 2012; Salkoff *et al.*, 2015; and Borgers, 2017). A disease with marked abnormalities in the gamma rhythm synchronization, schizophrenia, is known to have alterations in the synaptic strength, in particular, abnormalities in inhibition and in excitatory/inhibitory balance (e.g., Lewis *et al.*, 2005; Vierling-Claassen *et al.*, 2008; Lisman, 2012; Murray *et al.*, 2014; and Grent-'t-Jong *et al.*, 2018). Our study shows these abnormalities may not only affect the average synchronization strength, but may also affect the temporal patterning of synchrony, which, in turn, may affect how neural circuits process information (Ahn and Rubchinsky, 2013; 2017).

C. Some limitations of the study

There are several limitations of our modeling analysis that we would like to mention here. The model network is quite simple. Of course, no model is perfect, but it is important to remember that our model is a relatively small network while biologically realistic gamma probably requires large networks (Borgers *et al.*, 2012). Also, our model does not consider conduction delays, which may both promote and weaken synchronization (e.g., Woodman and Canavier, 2011). The signals we use here as a proxy for local field potentials are (necessarily) formed by a small number of neurons, which may be an issue both from the modeling perspective and from the time-series analysis perspective. The intermittent synchronized dynamics studied here naturally occurs in the network of oscillating units because the coupling strength is not very high. However, there may be other factors, which may contribute to the temporal variability of synchrony, such as the noise of different nature and synaptic plasticity (both are known to potentially affect temporal synchrony patterns, Zirkle and Rubchinsky, 2020, 2021). Nevertheless, given that the network expresses PING gamma, the results of the study are likely to be applicable to the gamma synchronization due to the pyramidal-interneuron gamma mechanism captured by this simple network.

D. Conclusion

We showed that synaptic changes may alter the temporal patterning of synchronization (and may do so independently of the synchronization strength) in the neural network exhibiting PING gamma rhythm. It was conjectured that this temporal patterning is physiologically important and that the dynamics with short desynchronizations may facilitate formation and breakup of transient neural assemblies (Ahn and Rubchinsky, 2013; 2017). Given the importance of gamma synchronization in facilitation of cognition and the short time scales associated with these phenomena, it is quite plausible that short desynchronization dynamics we observed in the PING gamma network is important for the formation of transient neural assemblies and for cognitive phenomena. Stronger local connections and weaker cross-circuit connections between inhibitory and excitatory neurons as well as weaker local and stronger cross-circuit connections between inhibitory and inhibitory neurons (which we found to promote short desynchronizations) may thus play a facilitatory role for these phenomena.

ACKNOWLEDGMENTS

This work was supported by the National Science Foundation (NSF) DMS (No. 1813819).

DATA AVAILABILITY

Data sharing is not applicable to this article as no new data were created or analyzed in this study.

REFERENCES

- Ahn, S. and Rubchinsky, L. L., "Short desynchronization episodes prevail in synchronous dynamics of human brain rhythms," *Chaos* **23**, 013138 (2013).
- Ahn, S. and Rubchinsky, L. L., "Potential mechanisms and functions of intermittent neural synchronization," *Front. Comput. Neurosci.* **11**, 44 (2017).
- Ahn, S., Park, C., and Rubchinsky, L. L., "Detecting the temporal structure of intermittent phase locking," *Phys. Rev. E: Stat., Nonlinear, Soft Matter Phys.* **84**, 016201 (2011).
- Ahn, S., Rubchinsky, L. L., and Lapiš, C. C., "Dynamical reorganization of synchronous activity patterns in prefrontal cortex-hippocampus networks during behavioral sensitization," *Cereb. Cortex* **24**, 2553–2561 (2014).
- Ahn, S., Zaubler, S. E., Witt, T., Worth, R. M., and Rubchinsky, L. L., "Neural synchronization: Average strength vs. temporal patterning," *Clin. Neurophysiol.* **129**, 842–844 (2018).
- Borgers, C., *An Introduction to Modeling Neuronal Dynamics* (Springer International Publishing, 2017).
- Borgers, C., Franzesi, G. T., Lebeau, F. E. N., Boyden, E., and Kopell, N., "Minimal size of cell assemblies coordinated by gamma oscillations," *PLoS Comput. Biol.* **8**, e1002362 (2012).
- Buzsáki, G., *Rhythms of the Brain* (Oxford University Press, 2006).
- Buzsáki, G. and Draguhn, A., "Neuronal oscillations in cortical networks," *Science* **304**, 1926–1929 (2004).
- Buzsáki, G. and Wang, X. J., "Mechanisms of gamma oscillations," *Annu. Rev. Neurosci.* **35**, 203–225 (2012).
- Dos Santos Lima, G. Z., Targa, A. D. S., de Freitas Cavalcante, S., Rodrigues, L. S., Fontenele-Araujo, J., Tortorolo, P., Andersen, M. L., and Lima, M. M. S., "Disruption of neocortical synchronisation during slow-wave sleep in the rotenone model of Parkinson's disease," *J. Sleep Res.* (published online, 2020).
- Ermentrout, G. B. and Kopell, N., "Fine structure of neural spiking and synchronization in the presence of conduction delays," *Proc. Natl. Acad. Sci. U.S.A.* **95**, 1259–1264 (1998).

- Ermentrout, G. B. and Terman, D. H., *Mathematical Foundations of Neuroscience* (Springer, New York, 2010).
- Fries, P., "Rhythms for cognition: Communication through coherence," *Neuron* **88**, 220–235 (2015).
- Grent-t-Jong, T., Gross, J., Goense, J., Wibral, M., Gajwani, R., Gumley, A. I., Lawrie, S. M., Schwannauer, M., Schultze-Lutter, F., Navarro, T., Koethe, D., Leweke, F. M., Singer, W., and Uhlhaas, P. J., "Resting-state gamma-band power alterations in schizophrenia reveal E/I-balance abnormalities across illness-stages," *Elife* **7**, e37799 (2018).
- Hammond, C., Bergmann, H., and Brown, P., "Pathological synchronization in Parkinson's disease: Networks, models, and treatments," *Trends Neurosci.* **30**, 357–364 (2007).
- Hurtado, J. M., Rubchinsky, L. L., and Sigvardt, K. A., "Statistical method for detection of phase-locking episodes in neural oscillations," *J. Neurophysiol.* **91**, 1883–1898 (2004).
- Izhikevich, E. M., *Dynamical Systems in Neuroscience: The Geometry of Excitability and Bursting* (MIT Press, Cambridge, MA, 2007).
- Lewis, D. A., Hashimoto, T., and Volk, D. W., "Cortical inhibitory neurons and schizophrenia," *Nat. Rev. Neurosci.* **6**, 312–324 (2005).
- Lisman, J., "Excitation, inhibition, local oscillations, or large-scale loops: What causes the symptoms of schizophrenia?," *Curr. Opin. Neurol.* **22**, 537–544 (2012).
- Malaia, E., Ahn, S., and Rubchinsky, L. L., "Dysregulation of temporal dynamics of synchronous neural activity in adolescents on autism spectrum," *Autism Res.* **13**, 24–31 (2020).
- Murray, J. D., Anticevic, A., Gancsos, M., Ichinose, M., Corlett, P. R., Krystal, J. H., and Wang, X. J., "Linking microcircuit dysfunction to cognitive impairment: Effects of disinhibition associated with schizophrenia in a cortical working memory model," *Cereb. Cortex* **24**, 859–872 (2014).
- Oswal, A., Brown, P., and Litvak, V., "Synchronized neural oscillations and the pathophysiology of Parkinson's disease," *Curr. Opin. Neurol.* **26**, 662–670 (2013).
- Park, C., Worth, R. M., and Rubchinsky, L. L., "Fine temporal structure of beta oscillations synchronization in subthalamic nucleus in Parkinson's disease," *J. Neurophysiol.* **103**, 2707–2716 (2010).
- Pikovsky, A., Rosenblum, M., and Kurths, J., *Synchronization: A Universal Concept in Nonlinear Sciences* (Cambridge University Press, Cambridge, 2001).
- Pittman-Polletta, B. R., Kocsis, B., Vijayan, S., Whittington, M. A., and Kopell, N. J., "Brain rhythms connect impaired inhibition to altered cognition in schizophrenia," *Biol. Psychiatry* **77**, 1020–1030 (2015).
- Ratnadurai-Giridharan, S., Zauber, S. E., Worth, R. M., Witt, T., Ahn, S., and Rubchinsky, L. L., "Temporal patterning of neural synchrony in the basal ganglia in Parkinson's disease," *Clin. Neurophysiol.* **127**, 1743–1745 (2016).
- Rubchinsky, L. L., Park, C., and Worth, R. M., "Intermittent neural synchronization in Parkinson's disease," *Nonlinear Dyn.* **68**, 329–346 (2012).
- Salkoff, D., Zaghera, E., Yüzgeç, Ö., and McCormick, D., "Synaptic mechanisms of tight spike synchrony at gamma frequency in cerebral cortex," *J. Neurosci.* **35**, 10236–10251 (2015).
- Spellman, T. J. and Gordon, J. A., "Synchrony in schizophrenia: A window into circuit-level pathophysiology," *Curr. Opin. Neurol.* **30**, 17–23 (2015).
- Sun, L., Grützner, C., Bölte, S., Wibral, M., Tozman, T., Schlitt, S., Poustka, F., Singer, W., Freitag, C.M., and Uhlhaas, P.J., "Impaired gamma-band activity during perceptual organization in adults with autism spectrum disorders: Evidence for dysfunctional network activity in frontal-posterior cortices," *J. Neuroscience* **32**(28), 9563–9573 (2012).
- Traub, R. D. and Miles, R., *Neuronal Networks of the Hippocampus* (Cambridge University Press, Cambridge, UK, 1991).
- Uhlhaas, P. J. and Singer, W., "Abnormal neural oscillations and synchrony in schizophrenia," *Nat. Rev. Neurosci.* **11**, 100–113 (2010).
- Vierling-Claassen, D., Siekmeier, P., Stufflebeam, S., and Kopell, N., "Modeling GABA alterations in schizophrenia: A link between impaired inhibition and altered gamma and beta range auditory entrainment," *J. Neurophysiol.* **99**, 2656–2671 (2008).
- Wang, X. J. and Buzsáki, G., "Gamma oscillation by synaptic inhibition in a hippocampal interneuronal network model," *J. Neurosci.* **16**, 6402–6413 (1996).
- Woodman, M. M. and Canavier, C. C., "Effects of conduction delays on the existence and stability of one to one phase locking between two pulse-coupled oscillators," *J. Comput. Neurosci.* **31**(2), 401–418 (2011).
- Zirkle, J. and Rubchinsky, L. L., "Spike-timing dependent plasticity effect on the temporal patterning of neural synchronization," *Front. Comput. Neurosci.* **14**, 52 (2020).
- Zirkle, Z. and Rubchinsky, L. L., "Noise effect on the temporal patterns of neural synchrony," *Neural Netw.* **141**, 30–39 (2021).